Planetesimal Accretion Beyond the Solar System: An Application to Systems of Tightly-Packed Inner Planets

Spencer Wallace

A dissertation
submitted in partial fulfillment of the
requirements for the degree of

Doctor of Philosophy

University of Washington

2023

Reading Committee:
Thomas Quinn, Chair
Rory Barnes
Eric Agol

Program Authorized to Offer Degree:
Astronomy

University of Washington

Abstract

Planetesimal Accretion Beyond the Solar System: An Application to Systems of Tightly-Packed Inner Planets

Spencer Wallace

Chair of the Supervisory Committee:
Chair Thomas Quinn
Department of Chair

This sample dissertation is an aid to students who are attempting to format their theses with LaTeX, a sophisticated text formatter widely used by mathematicians and scientists everywhere.

- It describes the use of a specialized macro package developed specifically for thesis production at the University. The macros customize LaTeX for the correct thesis style, allowing the student to concentrate on the substance of his or her text.[1]

- It demonstrates the solutions to a variety of formatting challenges found in thesis production.

- It serves as a template for a real dissertation.

[1]See Appendix A to obtain the source to this thesis and the class file.

TABLE OF CONTENTS

LIST OF FIGURES

ACKNOWLEDGMENTS

The author wishes to express sincere appreciation to University of Washington, where he has had the opportunity to work with the TEX formatting system, and to the author of TEX, Donald Knuth, *il miglior fabbro*.

DEDICATION

to my dear wife, Joanna

Chapter 1

INTRODUCTION

Chapter 2

FORMATION OF PLANETARY EMBRYOS IN THE INNER SOLAR SYSTEM

2.1 Introduction

The standard scenario of terrestrial planet formation involves the pairwise accretion of small rocky bodies, called planetesimals, that condense from dust out of the protostellar disc [76]. This accretion process can be broken into a series of distinct stages. First, dust particles settle toward the midplane of the disc and clump together via gravitational instability [23, 90], streaming instabilities [38, 37], turbulent concentration [10, 16, 15, 27] or direct sticking [67, 88, 20, 39]. These formation models predict a wide variation in the initial size of planetesimals, ranging from hundreds of meters up to a few hundred kilometers in diameter.

After this condensation process ends, growth continues via pairwise collisions between planetesimals. Above about 1 km in size, gravitational focusing becomes effective and the collision rate strongly increases. This marks the beginning of the intermediate stage of accretion. During this phase, runaway growth [19, 43, 5] quickly increases the size of the largest bodies. Eventually, the largest bodies grow massive enough to heat the small planetesimals, which then inhibits the runaway growth effect. This marks the transition into the phase of oligarchic growth in which the handful of large bodies all tend to grow at the same rate. This produces a bimodal size distribution of planetesimals, with many small bodies and a handful of very large bodies. During this phase, a combination of scattering events between the oligarchs and dynamical friction from the small planetesimals places the oligarchs on nearly circular orbits that are spaced apart by approximately 5-10 Hill radii [44]. Eventually, the oligarchs accrete most of the available material in the vicinity of their orbit, which eventually throttles their growth rate. On much longer time scales, the large bodies perturb

each other onto crossing orbits, forming Mars to Earth sized bodies via occasional collisions. This phase of late stage accretion is highly chaotic and takes much longer to play out than the previous stages [11, 72].

Generally, planetesimal accretion models fail to produce a configuration of planets that resembles that of the Solar System. Planets produced in the vicinity of Mars are systematically too massive [85, 71, 61, 34] and the terrestrial planets that form are too eccentric compared to their Solar System counterparts [11, 2, 9]. In addition, the present day water content of Earth, along with the large D/H ratio of Venus [18] does not match with models of solids that condensed out of the Solar nebula at 1 AU.

These issues all have proposed solutions, which generally involve altering the initial conditions for late-stage accretion simulations. The condition of the Solar System at the beginning of the late stage accretion phase is poorly constrained. This is mostly due to the fact that planetesimal formation, and therefore the intermediate accretion phase which produces the planetary embryos, is not well understood. Although the present day population of small Solar System bodies has continued to evolve since the end of the intermediate accretion phase, the current size frequency distribution (SFD) of asteroid belt and Kuiper belt objects contains some clues about the accretion history. [57] argued that the SFD of asteroid belt objects larger than 100 km in diameter has been largely unchanged, aside from a size independent depletion factor. [19] did a long term stability analysis of small Solar System objects and found that small bodies left over from accretion should still be largely unperturbed. For these reasons, it should be possible to connect observables in the Solar System to planetesimal formation theories by modeling only the intermediate stages of accretion.

There are two common ways to model planetesimal growth. A powerful approach is to use statistical methods to track the evolution of large groups of planetesimals. This is known as the particle-in-a-box method [24, 86]. The evolution of growth is followed by tracking planetesimals in discrete bins of mass and semi-major axis. This removes the need to calculate the motion of every individual body and allows very large collections of planetesimals to be followed. Unfortunately, the dynamics that governs the evolution of

these bodies does not always naturally emerge with this approach. As an example, [80] found that a careful treatment of three body encounters led to a different prediction for the initial size distribution of planetesimals near the asteroid belt. Additionally, the particle-in-a-box method is not well suited for studying oligarchic growth because the largest mass bins, which dominate the evolution in this stage, contain small numbers of bodies. Non-gravitational effects such as gas drag and fragmentation require extra care to implement self-consistently [49], although it has been successfully done [87, 9]. To alleviate some of these issues while still being able to model large populations, a newer hybrid approach, in which large bodies are treated as single entities and planetesimals are treated as statistical ensembles has been developed [82, 40, 51, 59].

The most reliable and straightforward approach is to use N-body methods to follow the evolution and growth of the planetesimals [48]. By tracking the individual motions of bodies, the dynamics governing their evolution naturally emerges, no matter what the distribution of bodies looks like. However, N-body simulations involving collision detection are extremely computationally expensive, which severely limits both the resolution and number of timesteps that can be achieved. This is why there are very few studies of runaway and oligarchic with direct N-body simulations in the literature [43, 44, 45, 5]. Instead, N-body methods are most commonly used to study late stage accretion, where the self-gravity and collisional evolution of the residual planetesimals is largely unimportant [11, 2, 9, 65, 57].

To date, we are not aware of any N-body simulations that resolve both the runaway and oligarchic growth phase with more than about 10^4 particles. At this resolution, stochasticity likely has a significant influence on dynamical friction and resonances may not be sufficiently resolved. [72] found that insufficient planetesimal resolution during the oligarchic growth phase limits the effectiveness of dynamical friction felt by the oligarchs, producing a population of embryos with unrealistically high eccentricities. This idea has also been applied to planet migration through a disc of planetesimals. [14] showed that resonances make a significant contribution to the dynamical friction torque exerted by the disc on the planet. This phenomenon requires the planetesimals to be finely resolved [8]. Dynamical friction

is also facilitated via resonances in galactic dynamics [54]. [84, 83] examined the effect of N-body particle counts on galaxy dynamics and showed that resonant interactions between the bar and halo were only effective with sufficient particle phase space coverage.

For these reasons, we motivate the need for a high resolution N-body simulation of planetesimal growth. We do this to better understand the effect that dynamical friction has on the intermediate stages of terrestrial planet growth and to examine what predictions a high resolution model makes about the residual population of planetesimals in the Solar System. In particular, resonances which are only effective with fine enough resolution, may have an important influence on planetesimal growth. In this paper, we investigate planetesimal evolution during the runaway and oligarchic growth phases with a direct N-body model. We begin by simulating an annulus of planetesimals with similar resolution to [44] to validate our model. We then run the same configuration with 100x more particles to better understand the effects of resolution on the intermediate stages of terrestrial planet growth.

In section 2.2, we describe the simulation code that we use and provide a detailed description of the collision model. We also summarize the initial conditions used. In section 2.3, we present the results of the low and high resolution simulation of terrestrial planet growth and highlight differences between the two. We find that a bump develops in the mass distribution of the high resolution simulation, which does not appear in the low resolution run. This feature manifests itself shortly after oligarchic growth commences and we infer that it is produced by extra heating via mean motion resonances between the oligarchs and small planetesimals. To further demonstrate this effect, we re-run the high resolution simulation with a narrower annulus (depopulating many of the resonances) and show that this reduces the prominence of the bump in the mass distribution. In section 2.4, we present a set of collisionless simulations of a planetary embryo embedded in an annulus of planetesimals. This more clearly demonstrates the differences in dynamical behavior between the low and high resolution models. In section **??**, we present two more simulations of planetesimal growth at intermediate resolutions and demonstrate that the location of the bump is sensitive to the initial planetesimal mass. Finally, section **??** connects these new results to our present

understanding of terrestrial planet growth and we discuss the additional steps necessary to use our results to constrain the initial size of planetesimals in the Solar System.

2.2 Simulations

2.2.1 Numerical Methods

All of the simulations described in this paper were performed with the highly parallel N-body code ChaNGa . ChaNGa is written in the CHARM++ programming language and has been shown to perform well when using up to half a million processors [55] simultaneously. Gravitational forces are calculated using a modified Barnes-Hut tree algorithm with hexadecapole order expansions of the moments. For all of the simulations described in this paper, a node opening criterion of $\Theta_{BH} = 0.7$ was used. [75] was able to resolve mean motion resonances in a terrestrial disc using a similar tree code with the same node opening criterion, so we expect that our model should properly handle resonance effects as well. The equations of motion are integrated using a kick-drift-kick leapfrog scheme. For more information about the implementation of ChaNGa see [36].

2.2.2 Collision Model

ChaNGa is a smoothed particle hydrodynamics code originally designed for cosmology simulations. In order to use ChaNGa to study planetesimal coagulation, we implemented a hard-body collision model that treats particles as solid objects with a fixed radius, rather than as smooth tracers of a fluid with a characteristic softening length. This work was largely based off of the hard body collision implementation in pkdgrav, which is described in [74] and [75].

Collisions are predicted at the beginning of each drift step by extrapolating the positions of the particles forward using the velocities calculated during the first kick. For each particle, the closest 64 neighbors are considered in the collision search. Because ChaNGa is a tree code, the nearest neighbors of a particle can be retrieved in $\mathcal{O}(N \log N)$ time. After

extrapolating the positions forward and checking for overlap with any neighbors, the earliest collision time t_{coll} is stored for each particle.

After the prediction phase, particles with t_{coll} less than the time step size ΔT must have their collisions resolved. For simplicity, all collisions in our simulations result in perfect accretion. [28] showed that excluding the effects of fragmentation and collisional rebound does not qualitatively change the growth modes of the planetesimals. A merger between two particles of mass m_1 and m_2 results in a single particle of mass $M = m_1 + m_2$, with the radius set to conserve density. The position and velocity of the resulting particle is set to the centre of mass position and velocity of the colliders at the moment of contact. The resulting merged particle is then drifted to the end of the step. If multiple collisions are predicted during a time step, the earliest collision is resolved first. Because resolving a collision can result in another imminent collision, collisions must be resolved one by one, with a new prediction check being run each time.

As in [43, 44] we accelerate the accretion process by artificially inflating the physical radius of the bodies by a factor of f. This technique reduces the accretion time-scale by approximately a factor of f^2, significantly reducing the number of timesteps that must be integrated. Additionally, inflating the particle radii allows us to use a smaller annulus with less planetesimals. The reason we cannot use an arbitrarily skinny annulus is because the edges tend to expand outward due to the unrealistic boundary conditions, decreasing the surface density. The time-scale for this expansion is set by the two body relaxation time-scale, which scales with N. Reducing the accretion time-scale by increasing f allows us to study planetesimal growth with a smaller, less computationally expensive annulus.

We must be careful, however, to choose a value of f that is not too large. The rms eccentricity and inclination of the planetesimal disc grows as gravitational encounters transform energy due to Keplerian shear into random motions. By accelerating the growth rate, we cause the transitions between growth modes to happen early, when the disc is less dynamically excited. This discrepancy is partly compensated for by the fact that our model ignores the effects of gas drag, which would damp the eccentricities and inclinations of the plan-

etesimals. We adopt $f = 6$ for our calculations, which reduces the amount of gravitational scattering by less than 10% of its true value and does not qualitatively change the modes of planetesimal growth [44].

As previously mentioned, simulation (ii) is meant to be compared with the results of [44]. This allows us to both validate our collision model and also have a baseline to compare our simulations to. In both cases, the planetesimals are distributed randomly in an annulus centred at 1 AU with a width $\Delta a = 0.085$ AU around a 1 $M_\odot$ star. This annulus width was chosen so that the required particle count is minimized without boundary effects influencing planetesimal growth. The surface mass density of the ring is set to 10 g cm^{-2}, which approximately corresponds to the minimum-mass solar nebula model [26] at 1 AU. In case (i), the eccentricities and inclinations are taken from a Rayleigh distribution [32] with $\langle e^2 \rangle^{1/2} = 2\langle i^2 \rangle^{1/2} = 4h/a$, where h is the mutual Hill radius. To match the same eccentricity and inclination dispersion with larger planetesimals in case (ii), we use $\langle e^2 \rangle^{1/2} = 2\langle i^2 \rangle^{1/2} = 0.635h/a$. In both simulations, the planetesimals are given an internal density of 2 g cm^{-3}. We use fixed timesteps with $\Delta T = 0.0025$ years and evolve the simulations for 20,000 years. Large timesteps diminish the effectiveness of gravitational focusing, which inhibits the collision rate. We find that the collision rate is converged below $\Delta T = 0.0025$ years. The integration time was chosen to be comparable to the orbital repulsion and Hill radius growth time-scale [42] so that the effects of oligarchic growth are fully realized by the end of the simulation.

It is worth noting that simulation (i) was a very computationally expensive undertaking. In total, the full 20,000 years of integration required approximately 130,000 CPU hours and over 50 days of wall clock time.

2.2.3 Initial Conditions

We begin by using our collision model to perform two sets of calculations:

(i) 10^6 equal mass bodies with $m = 1.2 \times 10^{21}$ g

(ii) 4000 equal mass bodies with $m = 3 \times 10^{23}$ g

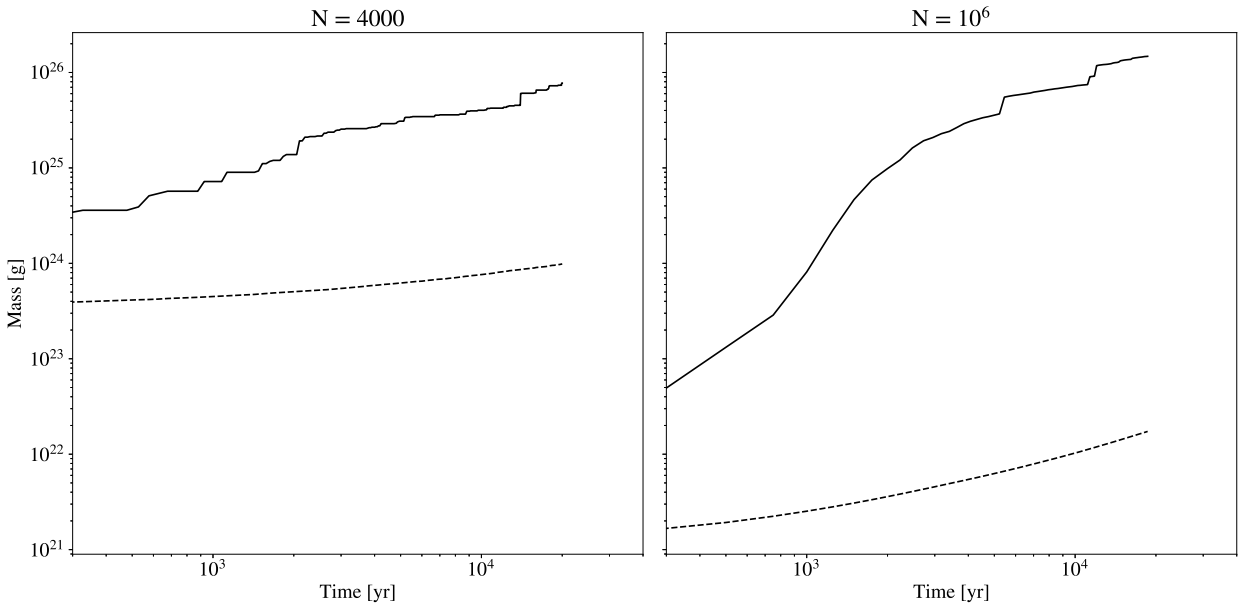

Figure 2.1: Evolution of the maximum (solid curve) and mean (dashed curve) planetesimal mass in the N=4000 and N=10^6 particle simulations. At early times, the maximum mass grows more quickly than the mean mass, which is indicative of runaway growth. After a few thousand years, the separation between the curves becomes a constant factor, signalling the start of oligarchic growth.

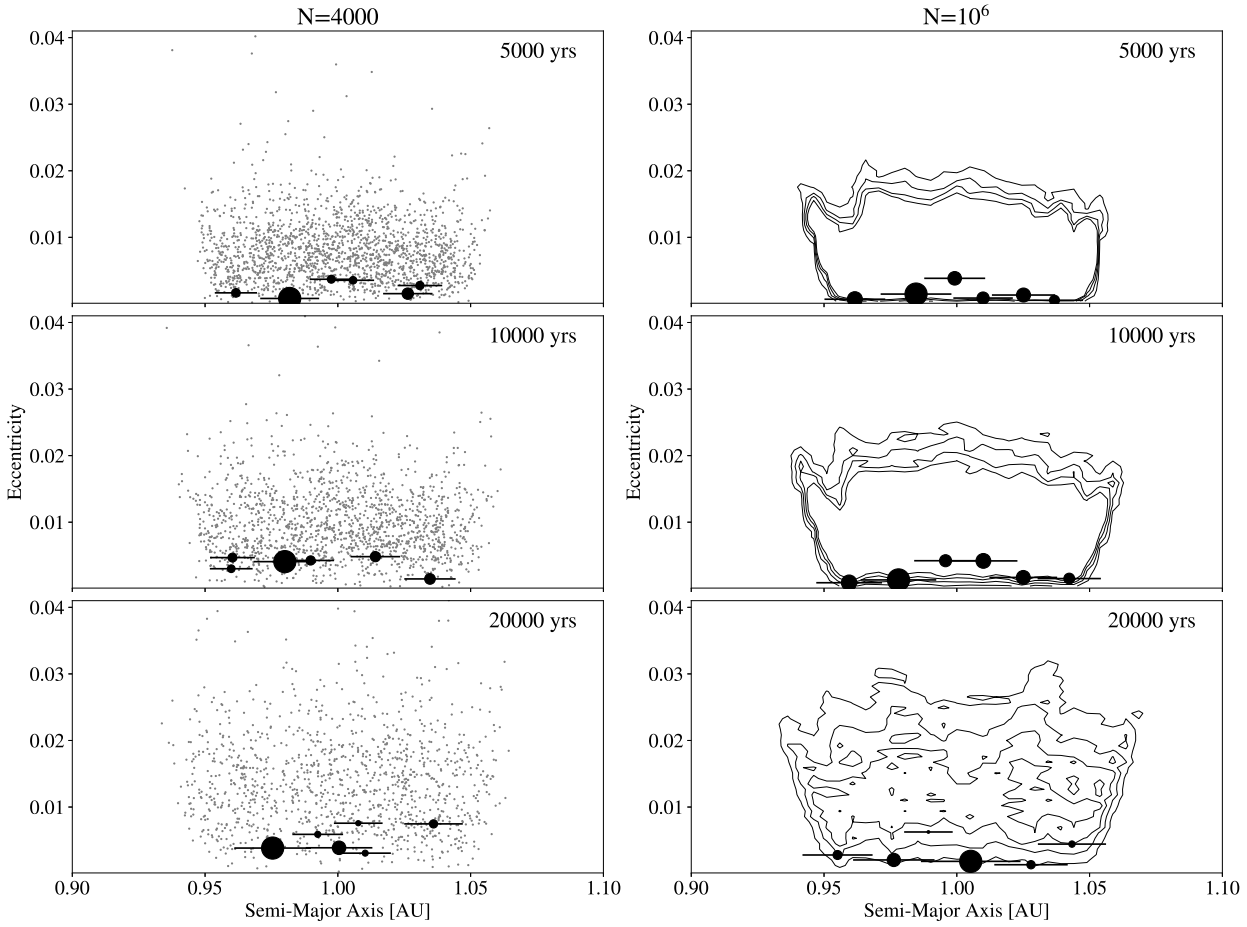

Figure 2.2: Snapshots from the low and high resolution models in the $a - e$ plane. On the left, the light dots represent individual planetesimals, while the contours on the right hand plots represent curves of constant number density. The contour levels are the same between all panels and correspond to 7.8×10^6, 1.6×10^7, 2.3×10^7, and 3.1×10^7 planetesimals per AU per unit eccentricity. The black circles denote the configuration of the 6 largest bodies in the simulation, with the area of the circles scaled to the mass of the body. The horizontal error bars are scaled to 5 times the Hill radius of the bodies.

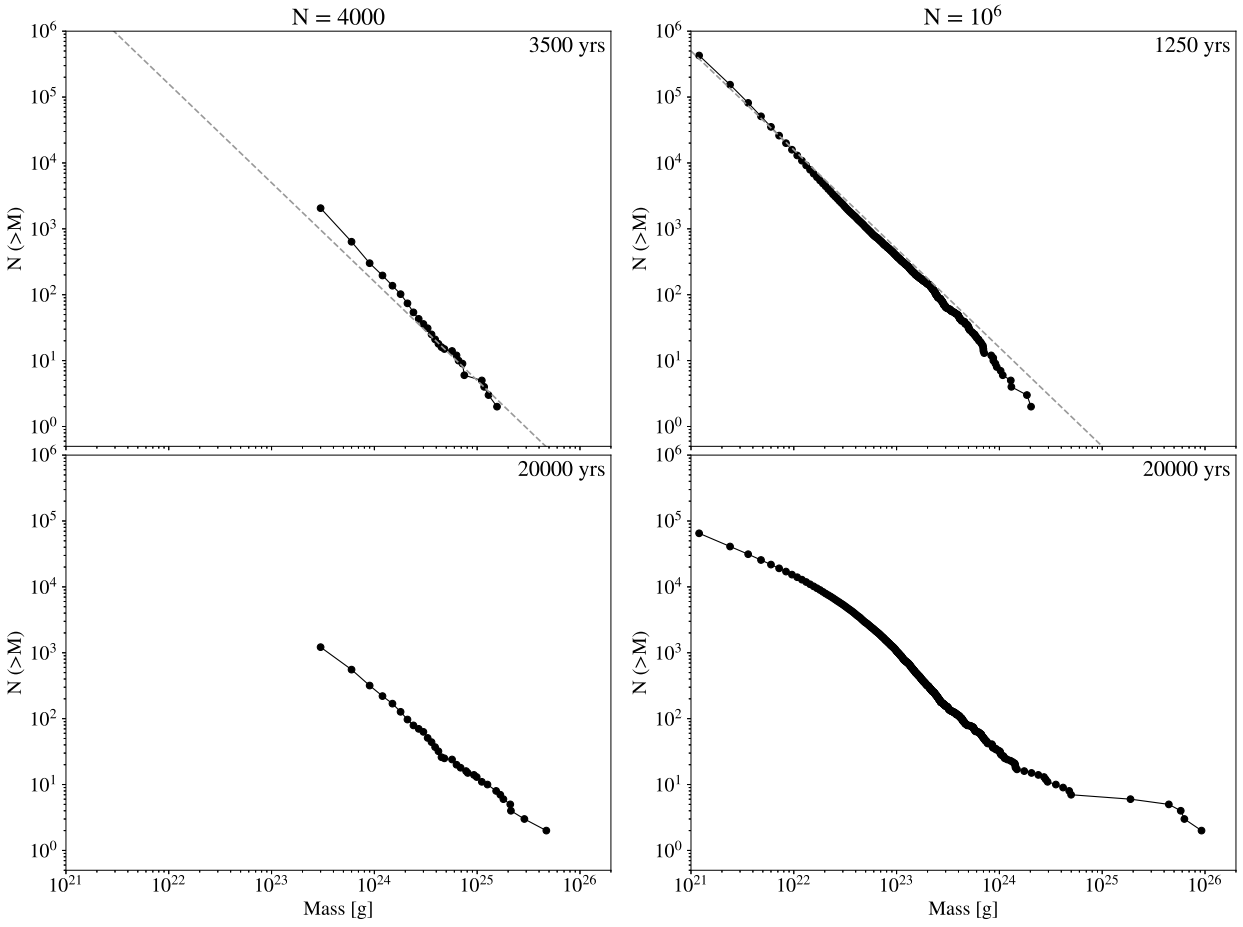

Figure 2.3: Cumulative number of bodies in each mass bin for the low and high resolution runs, shown at the end of runaway growth (top row) and the end of the simulation (bottom row). The dashed line indicates a slope of -1.5, which is characteristic of runaway growth.

2.3 Results

2.3.1 Low vs High Resolution

We begin by comparing the evolution of growth between the low resolution (N=4000) and high resolution (N=10^6) models. As planetesimals collide and grow, gravitational focusing becomes increasingly effective and the relative growth rate increases with mass [24]. Figure 2.1 shows the evolution of the average and maximum planetesimal mass in both simulations. Runaway growth at early times is evident from the fact that the maximum mass grows more quickly than the mean mass. Eventually, the largest bodies begin to dynamically heat the neighboring planetesimals, which slows the growth rate of the largest bodies.

When gravitational focusing and dynamical friction are both effective, the growth rate of a planetesimal of mass M is given by

$$\frac{dM}{dt} \propto \Sigma M^{4/3} e_m^{-2}, \tag{2.1}$$

where Σ is the surface density of solid material and e_m is the rms eccentricity of the planetesimals [42]. Before the oligarchs form, the eccentricity dispersion is independent of mass and the fractional growth rate scales like $dM/dt \propto M^{4/3}$ [87]. This implies that large bodies grow more quickly than small bodies, hence the runaway effect. Once the oligarchs form and dynamical friction becomes effective, energy equipartition causes the velocity dispersion to evolve toward $v_m \propto M^{-1/2}$[28]. Using $v_m \propto e_m$ [52], the growth rate during the oligarchic growth phase scales like $dM/dt \propto M^{2/3}$. Note that this does not imply that smaller bodies grow more quickly than large bodies. Rather, the growth rates tend towards the same value. This is reflected in figure 2.1, where the slope of the maximum mass curve flattens out to match the slope of the mean mass curve after a few thousand years.

Comparing the two panels in figure 2.1, it is also evident that the rate of growth is more vigorous in the high resolution case. This is due to the fact that the collision time-scale, given by

$$t_{coll} = \frac{1}{n\sigma v}, \tag{2.2}$$

is shorter in the latter case, where n is the number density of planetesimals, σ is the collision cross section and v is the typical encounter velocity. The collision cross section depends on both the geometric cross section ($\propto N^{-2/3}$) and an extra term due to gravitational focusing ($\propto N^{-7/3}$), where N is the total number of particles in the simulation and the total disk mass is fixed. Because the eccentricity and inclination dispersion (and therefore the scale height of the disk) are kept fixed between the low and high resolution simulations, the typical encounter velocity does not vary with N. Here, we retain only the leading order term for the collision cross section, in which case these quantities scale like $n \propto N$, $\sigma \propto N^{-2/3}$ and $v \propto const$ so that

$$t_{coll} \propto N^{-1/3}. \tag{2.3}$$

Figure 2.2 shows the a-e distribution of planetesimals at three snapshots from both simulations. In both cases, the eccentricity dispersion grows as energy from Keplerian shear is transformed into random motion, an effect known as viscous stirring [66]. The black circles denote the semi-major axis and eccentricity of the 6 largest bodies. The area of the circles indicates the mass of the bodies and the horizontal bars are each scaled to 5 times the Hill radius of the bodies. Gravitational scattering between the oligarchs, coupled with dynamical friction from the surrounding planetesimals, places the oligarchs on low eccentricity orbits that are spaced apart by a 5-10 Hill radii via orbital repulsion [44].

Next, we examine the evolution of the mass distribution of planetesimals. This is shown in figure 2.3. At early times, both models exhibit a power law distribution $N(< M) \propto m^{-p}$, where $p = 1.5$ for the small bodies. A mass distribution with this slope is characteristic of runaway growth [87]. The top panels show the mass distribution from both simulations at the end of the the runaway growth phase. In all subsequent snapshots, the mass distribution deviates from a single power law as the most massive bodies break away from the distribution,

signaling the start of oligarchic growth. This happens sooner in the high resolution case. The bottom panels show the mass distribution at the end of the simulation at T = 20,000 years.

Besides the fact that growth is more vigorous at higher resolution, the final mass distribution of planetesimals in the $N = 10^6$ case develops a feature that does not appear in the low resolution model. In the low resolution case, the low mass end of the mass distribution of planetesimals retains a single power law slope. The high resolution model, on the other hand, develops a bump in the mass distribution near 10^{22} g.

2.3.2 Explaining the Bump in the High Resolution Mass Spectrum

We would next like to determine what produces the feature at 10^{22} g in the high resolution simulation and why it is absent from the low resolution run. Upon close inspection of the simulation snapshots, both models retain a mass distribution that follows a single power law up until the onset of oligarchic growth. The bump in the high resolution mass spectrum becomes visible shortly after the oligarchs form. Over the course of the simulation, the bump gradually becomes more prominent. Because the bump appears shortly after the first oligarchs do, its presence is likely tied to the formation of the oligarchs.

Other investigations of planetesimal growth have revealed a similar bump in the size frequency distribution (SFD) at intermediate masses. [57] found that the location of this bump was set by the initial size of the planetesimals. Objects smaller than this size were created through disruptive collisions, which resulted in a shallower slope on the SFD to the left of the bump. Our collision model does not allow for fragmentation, so we must look for another explanation.

[**?**] showed that a bump in the SFD was an artefact of the transition between shear and dispersion dominated growth. Objects in the shear regime, whose encounter velocities are dominated by the differential rotation of the disc, grow more slowly than those in the dispersion regime, whose encounters are set by the random velocity dispersion. Because the velocity dispersion varies with planetesimal mass, both of these growth modes can operate

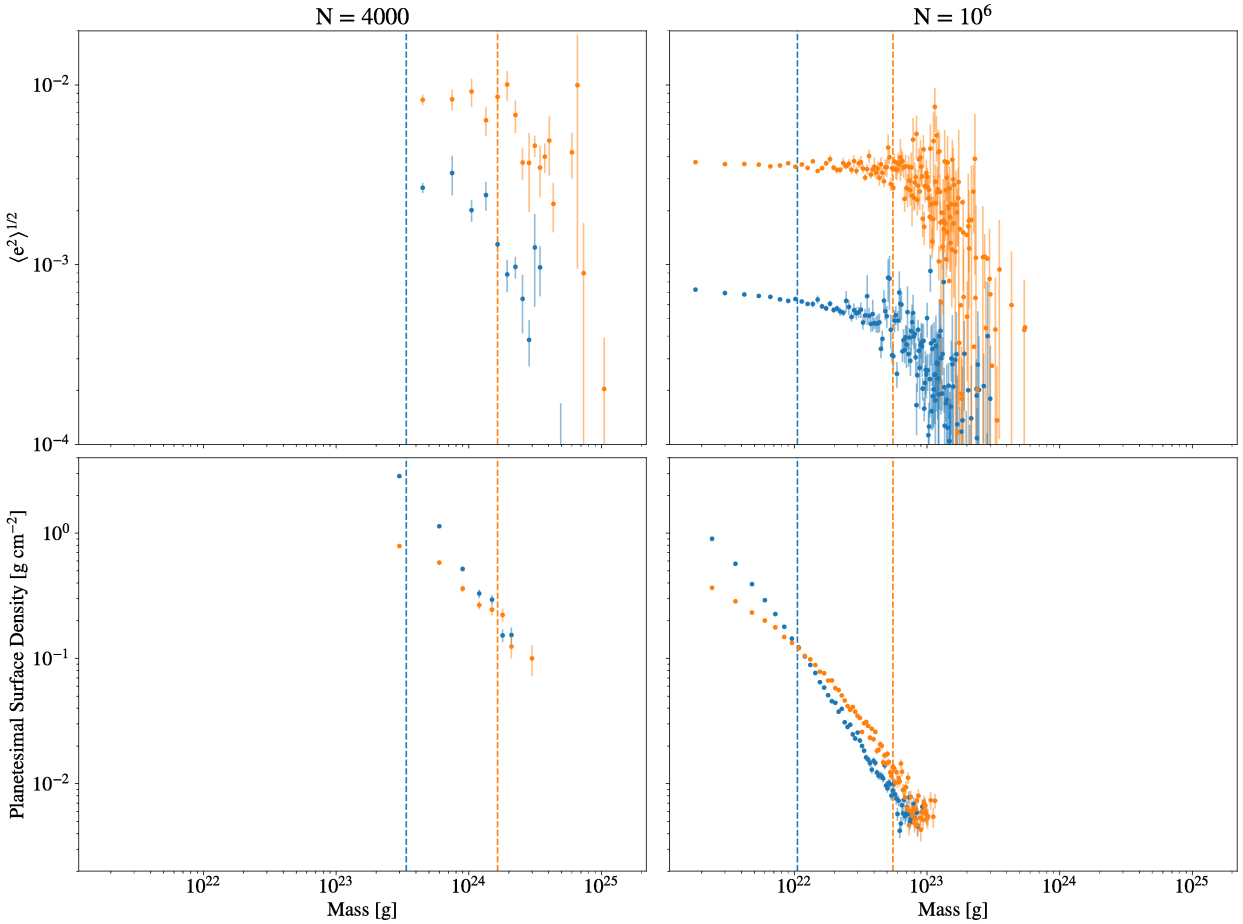

Figure 2.4: The rms eccentricity (top) and planetesimal surface density at each mass (bottom) shown for the $N = 4000$ and $N = 10^6$ simulations. The blue points correspond to the quantities at the end of the runaway growth phase (when the mass distribution deviates from a single power law) and the orange points are from the end of the simulations (T = 20,000 years). The vertical dashed lines indicate the value of M_{stir} during that snapshot.

simultaneously. Energy equipartition should cause the velocity dispersion to decrease with mass, so the transition between shear and dispersion dominated growth should happen at some intermediate mass. Finally, the smallest bodies have a velocity dispersion that exceeds their escape velocities, which sets a third, slow mode of growth in which gravitational focusing is ineffective. Although our high resolution simulation resolves all three modes of growth, we find that the boundaries between these modes smoothly and steadily evolve. Over the course of the simulation, the shear-dispersion boundary increases from about 10^{22} g to 10^{25} g, while the dispersion- escape boundary evolves from about 10^{21} to 10^{24} g. Any artefacts that these boundaries would leave on the planetesimal mass distribution should get washed out, so we also rule these out as explanations for the 10^{22} g bump.

Although the boundary between shear and dispersion dominated growth does not seem to be producing the bump, there still must be some kind of transition between growth modes occurring near this mass. As shown by equation 2.1, the growth rate is controlled by both the surface density of the planetesimals and their eccentricities. In figure 2.4, we show the rms eccentricity and surface mass density of the planetesimals as a function of mass at the end of the runaway growth phase (blue points) and at the end of the simulation (orange points). In this figure, each point corresponds to the relevant quantity calculated for all planetesimals with the exact same mass. Because the simulations start with equal mass planetesimals which grow via pairwise collisions, the masses take on discrete, linearly spaced values. We found that logarithmically binning the mass values alters the shape of the distributions, especially in the high resolution case where the quantities span many orders of magnitude. For this reason, we chose not to bin any of the data. The error bars in figure 2.4 are obtained via 10,000 iterations of bootstrap resampling. For the high resolution simulation, the error bars at low mass are smaller than the size of the points.

The surface density was determined by calculating an azimuthally averaged density profile using the analysis package PYNBODY [69]. The surface density for each planetesimal mass was taken to be the average surface density for those particles in a single radial bin from 0.9575 to 1.0425 AU, which spans the initial boundaries of the annulus.

One might expect that the rms eccentricity spectrum should eventually reach energy equipartition ($e \propto m^{-1/2}$), but this has been shown to only occur with a sufficiently steep mass distribution [70]. In our case, the mass distribution is shallow enough that the velocity evolution of the low mass bodies is set only by interactions with large planetesimals. The mass below which this occurs, shown by the vertical dashed lines in figure 2.4 is given by [87, 68]

$$M_{stir} = \frac{\langle m^2 \rangle}{\langle m \rangle}. \tag{2.4}$$

Below this mass, planetesimals do not produce a dynamical friction wake and their velocity evolution becomes independent of mass [70]. Because we started with equal mass planetesimals, the mass distribution was steep at early times. A power law slope steeper than $p = -2$ should produce a mass-dependent velocity distribution everywhere [70]. In the top right panel of figure 2.4, the rms eccentricity distribution is not entirely flat below M_{stir}, which is likely due to the evolving mass spectrum. The analysis of [70], however, assumes a static mass spectrum.

At late times, a power law break in the surface density distribution forms near 10^{22} g in the high resolution simulation. Because the surface density is tied to both the mass distribution and the spatial distribution of planetesimals, it is difficult to learn anything else about the dynamics that are altering the growth rate from this information alone. We will examine this further in section **??**.

Given the power law break in the surface density distribution below 10^{22} g, we infer that there must be a dynamical mechanism at work that alters the collision rates of the low mass bodies. By the time that the 10^{22} g bump begins to appear, the planetesimals are sufficiently hot enough to render gravitational focusing ineffective (equation 2.1 is also no longer applicable). In this case, any additional heating actually increases the collision rate. Because this effect appears around the time of the onset of oligarchic growth, it likely has something to do with dynamical friction between the oligarchs and the planetesimals. In the next section, we examine how dynamical friction might be more effective with small

planetesimals.

2.4 Dynamical Friction and Resolution

Although the Chandrasekhar formula [12] contains no dependence on particle mass, the 'granularity' of the surrounding medium has been shown to influence the action of dynamical friction [8]. This is because the individual kicks from gravitational encounters become less frequent and more powerful at coarse resolution, introducing extra stochasticity as the system evolves toward energy equipartition. [65] showed that a finely resolved planetesimal distribution during the oligarchic growth phase produced planetary embryos with low eccentricities. They did not, however, examine the mass spectrum to see if the oligarchs were preferentially heating the smallest planetesimals. In addition, their simulations only contained a few thousand particles, while our high resolution run contains in excess of 200,000 bodies at the onset of oligarchic growth. Comparing the largest embryos at the end of simulation (i) to their results, we find that the largest embryo in our high resolution run has an eccentricity that is a factor of 2 smaller than the embryos produced by [65].

In addition to altering the cumulative effect of close gravitational encounters, there is evidence that energy and angular momentum exchange through resonances is more effective with fine granularity. For example, in collisionless simulations of galaxies, [84, 83] showed that a minimum number of particles was required to populate resonances and couple the rotation of a bar to the central halo cusp through Lindblad resonances. If the resolution was too coarse, gravitational potential fluctuations would scatter particles out of resonances and prevent any strong torque between the bar and the halo. Likewise, [14] showed that resonant torque has a measurable effect on the interaction between a planet and a planetesimal disc.

2.4.1 Resolved Resonances

During the oligarchic growth phase, a handful of massive bodies lose energy and angular momentum to the surrounding medium. The previous runaway growth phase leaves behind a steadily varying spectrum of planetesimal masses, whose number decreases with mass.

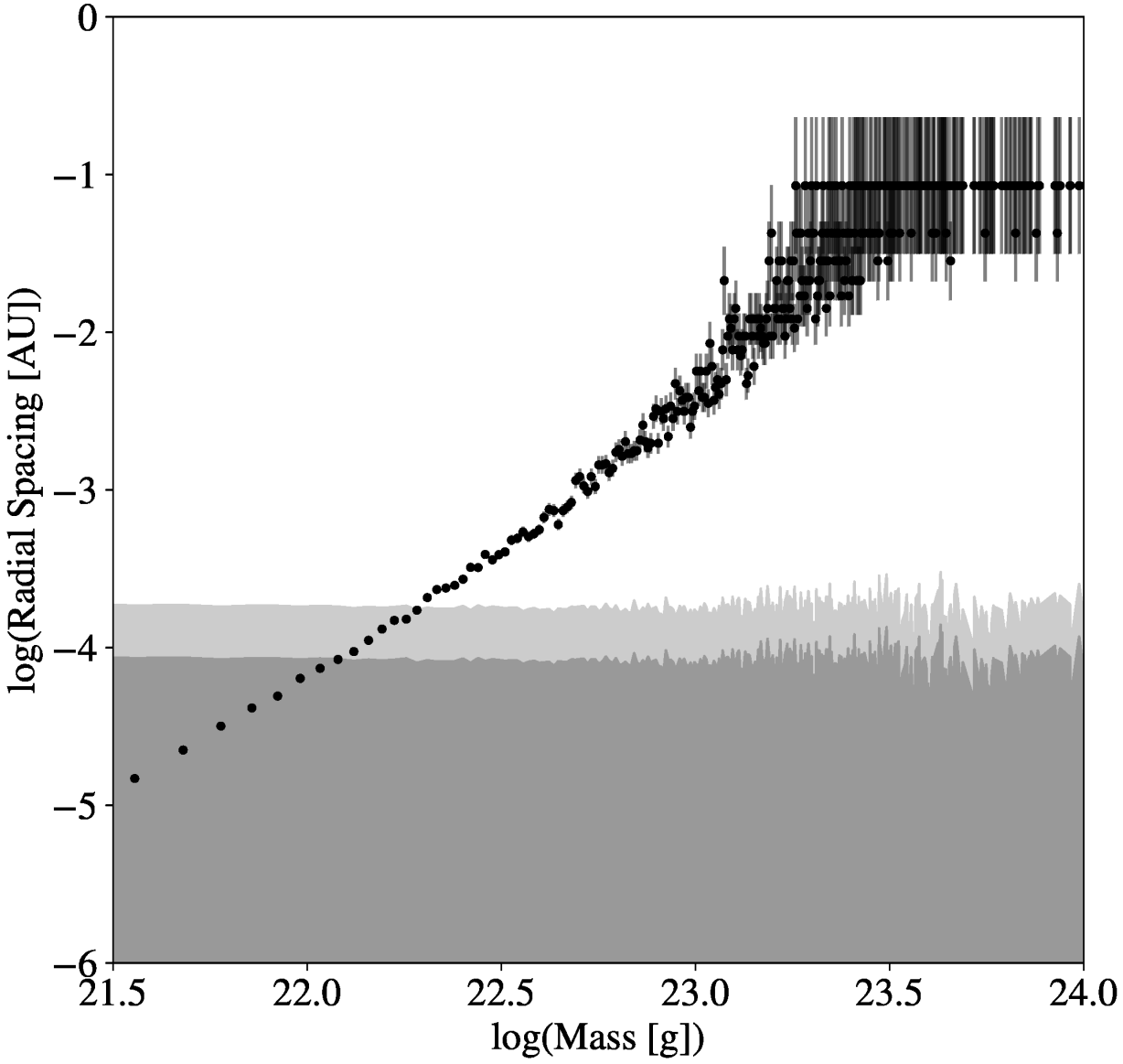

Figure 2.5: The average spacing in semi-major axis as a function of mass at the end of the high resolution growth simulation (black points). The gray regions indicate the libration width of planetesimals in each mass bin that are in resonance with the most massive oligarch. The light gray region corresponds to the libration width of the 65:64 (highest non-overlapping) resonance and the dark gray region corresponds to the 15:14 (most distant populated) resonance.

Assuming the planetesimals are randomly distributed throughout the disc, the granularity can be thought of as increasing with mass. This implies that the dynamical friction should be more effective from the smallest planetesimals. Because the planetesimals appear to be more strongly heated below a certain mass threshold, we hypothesize that the change in growth modes has to do with the activation of resonances, rather than a smooth decrease in the stochasticity of scattering events.

Because spiral features like those seen in [84, 83] and [14] are unlikely to form in such a narrow annulus, we will consider the effects of mean motion resonances (MMRs), which are a subset of the Lindblad resonances considered in the aforementioned studies. In order to determine the resolution required to resolve MMRs, we calculate the libration width of first order MMRs associated with the oligarchs and compare it to the average radial spacing between planetesimals as a function mass. The average radial spacing is given by

$$\langle \Delta r \rangle = \frac{\Delta a}{N(m)}, \tag{2.5}$$

where Δa is the width of the annulus and $N(m)$ is the number of planetesimals of each mass.

Chapter 3

DETECTING COLD JUPITERS VIA COLLISIONAL GRINDING OF PLANETESIMALS

Chapter 4

FORMATION OF PLANETARY EMBRYOS AT SHORT ORBITAL PERIODS

Chapter 5

IN-SITU FORMATION OF STIPS

BIBLIOGRAPHY

[1] I. Adachi, C. Hayashi, and K. Nakazawa. The gas drag effect on the elliptical motion of a solid body in the primordial solar nebula. *Progress of Theoretical Physics*, 56:1756–1771, December 1976.

[2] C. B. Agnor, R. M. Canup, and H. F. Levison. On the Character and Consequences of Large Impacts in the Late Stage of Terrestrial Planet Formation. *Icarus*, 142:219–237, November 1999.

[3] Y. Alibert, C. Mordasini, W. Benz, and C. Winisdoerffer. Models of giant planet formation with migration and disc evolution. *A&A*, 434(1):343–353, Apr 2005.

[4] P. J. Armitage. *Astrophysics of Planet Formation*. October 2013.

[5] R. Barnes, T. R. Quinn, J. J. Lissauer, and D. C. Richardson. N-Body simulations of growth from 1 km planetesimals at 0.4 AU. *Icarus*, 203:626–643, October 2009.

[6] C. Baruteau, A. Crida, S. J. Paardekooper, F. Masset, J. Guilet, B. Bitsch, R. Nelson, W. Kley, and J. Papaloizou. Planet-Disk Interactions and Early Evolution of Planetary Systems. In Henrik Beuther, Ralf S. Klessen, Cornelis P. Dullemond, and Thomas Henning, editors, *Protostars and Planets VI*, page 667, Jan 2014.

[7] W. F. Bottke, D. D. Durda, D. Nesvorný, R. Jedicke, A. Morbidelli, D. Vokrouhlický, and H. Levison. The fossilized size distribution of the main asteroid belt. *Icarus*, 175:111–140, May 2005.

[8] Adrián Brunini, Pablo J. Santamaría, Héctor R. Viturro, and Rodolfo G. Cionco. On the number of particles in N-body simulations of planet disk interaction. *Planetary and Space Science*, 55:2121–2127, November 2007.

[9] J. E. Chambers. Making More Terrestrial Planets. *Icarus*, 152:205–224, August 2001.

[10] J. E. Chambers. Planetesimal formation by turbulent concentration. *Icarus*, 208:505–517, August 2010.

[11] J. E. Chambers and G. W. Wetherill. Making the Terrestrial Planets: N-Body Integrations of Planetary Embryos in Three Dimensions. *Icarus*, 136:304–327, December 1998.

[12] S. Chandrasekhar. Dynamical Friction. I. General Considerations: the Coefficient of Dynamical Friction. *ApJ*, 97:255, March 1943.

[13] Subrahmanyan Chandrasekhar. *Principles of stellar dynamics*. 1960.

[14] R. G. Cionco and A. Brunini. Orbital migrations in planetesimal discs: N-body simulations and the resonant dynamical friction. *MNRAS*, 334:77–86, July 2002.

[15] J. N. Cuzzi, R. C. Hogan, and W. F. Bottke. Towards initial mass functions for asteroids and Kuiper Belt Objects. *Icarus*, 208:518–538, August 2010.

[16] J. N. Cuzzi, R. C. Hogan, and K. Shariff. Toward Planetesimals: Dense Chondrule Clumps in the Protoplanetary Nebula. *ApJ*, 687:1432–1447, November 2008.

[17] Stanley F. Dermott, Renu Malhotra, and Carl D. Murray. Dynamics of the Uranian and Saturnian satelite systems: A chaotic route to melting Miranda? *Icarus*, 76(2):295–334, Nov 1988.

[18] T. M. Donahue, J. H. Hoffman, R. R. Hodges, and A. J. Watson. Venus was wet - A measurement of the ratio of deuterium to hydrogen. *Science*, 216:630–633, May 1982.

[19] M. Duncan, T. Quinn, and S. Tremaine. The long-term evolution of orbits in the solar system - A mapping approach. *Icarus*, 82:402–418, December 1989.

[20] P. Garaud, F. Meru, M. Galvagni, and C. Olczak. From Dust to Planetesimals: An Improved Model for Collisional Growth in Protoplanetary Disks. *ApJ*, 764:146, February 2013.

[21] P. Goldreich and S. Tremaine. The excitation of density waves at the Lindblad and corotation resonances by an external potential. *ApJ*, 233:857–871, Nov 1979.

[22] P. Goldreich and S. Tremaine. Disk-satellite interactions. *ApJ*, 241:425–441, Oct 1980.

[23] P. Goldreich and W. R. Ward. The Formation of Planetesimals. *ApJ*, 183:1051–1062, August 1973.

[24] R. Greenberg, W. K. Hartmann, C. R. Chapman, and J. F. Wacker. Planetesimals to planets - Numerical simulation of collisional evolution. *Icarus*, 35:1–26, July 1978.

[25] Evgeni Grishin and Hagai B. Perets. Application of Gas Dynamical Friction for Planetesimals. I. Evolution of Single Planetesimals. *ApJ*, 811:54, Sep 2015.

[26] C. Hayashi. Structure of the Solar Nebula, Growth and Decay of Magnetic Fields and Effects of Magnetic and Turbulent Viscosities on the Nebula. *Progress of Theoretical Physics Supplement*, 70:35–53, 1981.

[27] P. F. Hopkins. Jumping the gap: the formation conditions and mass function of 'pebble-pile' planetesimals. *MNRAS*, 456:2383–2405, March 2016.

[28] S. Ida, E. Kokubo, and J. Makino. The Origin of Anisotropic Velocity Dispersion of Particles in a Disc Potential. *MNRAS*, 263:875, Aug 1993.

[29] S. Ida and D. N. C. Lin. Toward a Deterministic Model of Planetary Formation. I. A Desert in the Mass and Semimajor Axis Distributions of Extrasolar Planets. *ApJ*, 604(1):388–413, Mar 2004.

[30] S. Ida and J. Makino. Scattering of planetesimals by a protoplanet - Slowing down of runaway growth. *Icarus*, 106:210, November 1993.

[31] Shigeru Ida, Geoffrey Bryden, D. N. C. Lin, and Hidekazu Tanaka. Orbital Migration of Neptune and Orbital Distribution of Trans-Neptunian Objects. *ApJ*, 534(1):428–445, May 2000.

[32] Shigeru Ida and Junichiro Makino. N-Body simulation of gravitational interaction between planetesimals and a protoplanet . I. velocity distribution of planetesimals. *Icarus*, 96:107–120, March 1992.

[33] Satoshi Inaba, Hidekazu Tanaka, Kiyoshi Nakazawa, George W. Wetherill, and Eiichiro Kokubo. High-Accuracy Statistical Simulation of Planetary Accretion: II. Comparison with N-Body Simulation. *Icarus*, 149(1):235–250, Jan 2001.

[34] A. Izidoro, S. N. Raymond, A. Morbidelli, and O. C. Winter. Terrestrial planet formation constrained by Mars and the structure of the asteroid belt. *MNRAS*, 453:3619–3634, November 2015.

[35] R. Jedicke, J. Larsen, and T. Spahr. *Observational Selection Effects in Asteroid Surveys*, pages 71–87. 2002.

[36] P. Jetley, F. Gioachin, L. Mendes, C. Kale, and T. Quinn. Massively parallel cosmological simulations with ChaNGa. *Proceedings of IEEE International Parallel and Distributed Processing Symposium*, 2008.

[37] A. Johansen, M.-M. Mac Low, P. Lacerda, and M. Bizzarro. Growth of asteroids, planetary embryos, and Kuiper belt objects by chondrule accretion. *Science Advances*, 1:1500109, April 2015.

[38] A. Johansen, J. S. Oishi, M.-M. Mac Low, H. Klahr, T. Henning, and A. Youdin. Rapid planetesimal formation in turbulent circumstellar disks. *Nature*, 448:1022–1025, August 2007.

[39] A. Kataoka, H. Tanaka, S. Okuzumi, and K. Wada. Fluffy dust forms icy planetesimals by static compression. *A&A*, 557:L4, September 2013.

[40] Scott J. Kenyon and Benjamin C. Bromley. Terrestrial Planet Formation. I. The Transition from Oligarchic Growth to Chaotic Growth. *AJ*, 131(3):1837–1850, Mar 2006.

[41] David R. Kirsh, Martin Duncan, Ramon Brasser, and Harold F. Levison. Simulations of planet migration driven by planetesimal scattering. *Icarus*, 199(1):197–209, Jan 2009.

[42] E. Kokubo and S. Ida. Orbital evolution of protoplanets embedded in a swarm of planetesimals. *Icarus*, 114:247–257, April 1995.

[43] E. Kokubo and S. Ida. On Runaway Growth of Planetesimals. *Icarus*, 123:180–191, September 1996.

[44] E. Kokubo and S. Ida. Oligarchic Growth of Protoplanets. *Icarus*, 131:171–178, January 1998.

[45] E. Kokubo and S. Ida. Formation of Protoplanet Systems and Diversity of Planetary Systems. *ApJ*, 581:666–680, December 2002.

[46] E. Kokubo and S. Ida. Dynamics and accretion of planetesimals. *Progress of Theoretical and Experimental Physics*, 2012(1):01A308, October 2012.

[47] Eiichiro Kokubo and Shigeru Ida. Formation of Protoplanets from Planetesimals in the Solar Nebula. *Icarus*, 143:15–27, January 2000.

[48] M. Lecar and S. J. Aarseth. A numerical simulation of the formation of the terrestrial planets. *ApJ*, 305:564–579, June 1986.

[49] Z. M. Leinhardt. Terrestrial Planet Formation: A Review and Current Directions. In D. Fischer, F. A. Rasio, S. E. Thorsett, and A. Wolszczan, editors, *Extreme Solar Systems*, volume 398 of *Astronomical Society of the Pacific Conference Series*, page 225, 2008.

[50] Z. M. Leinhardt and D. C. Richardson. Planetesimals to Protoplanets. I. Effect of Fragmentation on Terrestrial Planet Formation. *ApJ*, 625:427–440, May 2005.

[51] H. F. Levison, M. J. Duncan, and E. Thommes. A Lagrangian Integrator for Planetary Accretion and Dynamics (LIPAD). *AJ*, 144:119, October 2012.

[52] Jack J. Lissauer and Glen R. Stewart. Growth of Planets from Planetesimals. In Eugene H. Levy and Jonathan I. Lunine, editors, *Protostars and Planets III*, page 1061, Jan 1993.

[53] Y. Lithwick. After Runaway: The Trans-Hill Stage of Planetesimal Growth. *ApJ*, 780:22, January 2014.

[54] D. Lynden-Bell and A. J. Kalnajs. On the generating mechanism of spiral structure. *MNRAS*, 157:1, January 1972.

[55] H. Menon, L. Wesolowski, and G. et al. Zheng. Adaptive Techniques for Clustered N-Body Cosmological Simulations. *Computational Astrophysics and Cosmology*, 2:1, 2015.

[56] Y. Miguel, O. M. Guilera, and A. Brunini. The diversity of planetary system architectures: contrasting theory with observations. *MNRAS*, 417(1):314–332, Oct 2011.

[57] A. Morbidelli, W. F. Bottke, D. Nesvorný, and H. F. Levison. Asteroids were born big. *Icarus*, 204:558–573, December 2009.

[58] A. Morbidelli, J. I. Lunine, D. P. O'Brien, S. N. Raymond, and K. J. Walsh. Building Terrestrial Planets. *Annual Review of Earth and Planetary Sciences*, 40:251–275, May 2012.

[59] R. Morishima. A particle-based hybrid code for planet formation. *Icarus*, 260:368–395, November 2015.

[60] R. Morishima. Onset of oligarchic growth and implication for accretion histories of dwarf planets. *Icarus*, 281:459–475, January 2017.

[61] R. Morishima, J. Stadel, and B. Moore. From planetesimals to terrestrial planets: N-body simulations including the effects of nebular gas and giant planets. *Icarus*, 207:517–535, June 2010.

[62] C. D. Murray and S. F. Dermott. *Solar System Dynamics*. February 2000.

[63] R. A. Murray-Clay and E. I. Chiang. Brownian Motion in Planetary Migration. *ApJ*, 651:1194–1208, November 2006.

[64] Y. Nakagawa, M. Sekiya, and C. Hayashi. Settling and growth of dust particles in a laminar phase of a low-mass solar nebula. *Icarus*, 67:375–390, September 1986.

[65] D. P. O'Brien, A. Morbidelli, and H. F. Levison. Terrestrial planet formation with strong dynamical friction. *Icarus*, 184:39–58, September 2006.

[66] K. Ohtsuki, G. R. Stewart, and S. Ida. Evolution of Planetesimal Velocities Based on Three-Body Orbital Integrations and Growth of Protoplanets. *Icarus*, 155:436–453, February 2002.

[67] S. Okuzumi, H. Tanaka, H. Kobayashi, and K. Wada. Rapid Coagulation of Porous Dust Aggregates outside the Snow Line: A Pathway to Successful Icy Planetesimal Formation. *ApJ*, 752:106, June 2012.

[68] C. W. Ormel, C. P. Dullemond, and M. Spaans. Accretion among preplanetary bodies: The many faces of runaway growth. *Icarus*, 210:507–538, November 2010.

[69] Andrew Pontzen, Rok Roškar, Greg Stinson, and Rory Woods. pynbody: N-Body/SPH analysis for python. Astrophysics Source Code Library, May 2013.

[70] R. R. Rafikov. Dynamical Evolution of Planetesimals in Protoplanetary Disks. *AJ*, 126:2529–2548, November 2003.

[71] S. N. Raymond, D. P. O'Brien, A. Morbidelli, and N. A. Kaib. Building the terrestrial planets: Constrained accretion in the inner Solar System. *Icarus*, 203:644–662, October 2009.

[72] S. N. Raymond, T. Quinn, and J. I. Lunine. High-resolution simulations of the final assembly of Earth-like planets I. Terrestrial accretion and dynamics. *Icarus*, 183:265–282, August 2006.

[73] Sean N. Raymond, Thomas Quinn, and Jonathan I. Lunine. Making other earths: dynamical simulations of terrestrial planet formation and water delivery. *Icarus*, 168:1–17, March 2004.

[74] D. C. Richardson. Tree Code Simulations of Planetary Rings. *MNRAS*, 269:493, July 1994.

[75] D. C. Richardson, T. Quinn, J. Stadel, and G. Lake. Direct Large-Scale N-Body Simulations of Planetesimal Dynamics. *Icarus*, 143:45–59, January 2000.

[76] V. S. Safronov and E. V. Zvjagina. Relative Sizes of the Largest Bodies during the Accumulation of Planets. *Icarus*, 10:109–115, January 1969.

[77] A. Shannon, Y. Wu, and Y. Lithwick. Conglomeration of Kilometer-sized Planetesimals. *ApJ*, 801:15, March 2015.

[78] Hidekazu Tanaka, Taku Takeuchi, and William R. Ward. Three-Dimensional Interaction between a Planet and an Isothermal Gaseous Disk. I. Corotation and Lindblad Torques and Planet Migration. *ApJ*, 565(2):1257–1274, Feb 2002.

[79] S. J. Weidenschilling. Aerodynamics of solid bodies in the solar nebula. *MNRAS*, 180:57–70, July 1977.

[80] S. J. Weidenschilling. Initial sizes of planetesimals and accretion of the asteroids. *Icarus*, 214:671–684, August 2011.

[81] S. J. Weidenschilling and D. R. Davis. Orbital resonances in the solar nebula: Implications for planetary accretion. *Icarus*, 62(1):16–29, Apr 1985.

[82] S. J. Weidenschilling, D. Spaute, D. R. Davis, F. Marzari, and K. Ohtsuki. Accretional Evolution of a Planetesimal Swarm. *Icarus*, 128(2):429–455, Aug 1997.

[83] M. D. Weinberg and N. Katz. The bar-halo interaction - II. Secular evolution and the religion of N-body simulations. *MNRAS*, 375:460–476, February 2007.

[84] Martin D. Weinberg and Neal Katz. The bar-halo interaction - I. From fundamental dynamics to revised N-body requirements. *MNRAS*, 375(2):425–459, February 2007.

[85] G. W. Wetherill. An alternative model for the formation of the asteroids. *Icarus*, 100:307–325, December 1992.

[86] G. W. Wetherill and G. R. Stewart. Accumulation of a swarm of small planetesimals. *Icarus*, 77:330–357, February 1989.

[87] G. W. Wetherill and G. R. Stewart. Formation of planetary embryos - Effects of fragmentation, low relative velocity, and independent variation of eccentricity and inclination. *Icarus*, 106:190, November 1993.

[88] F. Windmark, T. Birnstiel, C. Güttler, J. Blum, C. P. Dullemond, and T. Henning. Planetesimal formation by sweep-up: how the bouncing barrier can be beneficial to growth. *A&A*, 540:A73, April 2012.

[89] O. C. Winter and C. D. Murray. Resonance and chaos. I. First-order interior resonances. *A&A*, 319:290–304, March 1997.

[90] A. N. Youdin and F. H. Shu. Planetesimal Formation by Gravitational Instability. *ApJ*, 580:494–505, November 2002.

Appendix A

WHERE TO FIND THE FILES

The uwthesis class file, `uwthesis.cls`, contains the parameter settings, macro definitions, and other TEXnical commands which allow LATEX to format a thesis. The source to the document you are reading, `uwthesis.tex`, contains many formatting examples which you may find useful. The bibliography database, `uwthesis.bib`, contains instructions to BibTeX to create and format the bibliography. You can find the latest of these files on:

- My page.

  `https://staff.washington.edu/fox/tex/thesis.shtml`

- CTAN

  `http://tug.ctan.org/tex-archive/macros/latex/contrib/uwthesis/`

  (not always as up-to-date as my site)

VITA

Jim Fox is a Software Engineer with IT Infrastructure Division at the University of Washington. His duties do not include maintaining this package. That is rather an avocation which he enjoys as time and circumstance allow.

He welcomes your comments to `fox@uw.edu`.